Chinese Chemical Letters 32 (2021) 1215–1219

Contents lists available at ScienceDirect

Chinese Chemical Letters

journal homepage: www.elsevier.com/locate/cclet

Communication

Synergistic *in-situ* growth of silver nanoparticles with nanozyme activity for dual-mode biosensing and cancer theranostics

Xin Hai[a], Yuwei Li[a], Kaixin Yu[a], Shuzhen Yue[a], Yuanfang Li[a], Weiling Song[c], Sai Bi[a,*], Xueji Zhang[b,*]

[a] *Research Center for Intelligent and Wearable Technology, College of Chemistry and Chemical Engineering, Qingdao University, Qingdao 266071, China*
[b] *School of Biomedical Engineering, Shenzhen University Health Science Center, Shenzhen 518060, China*
[c] *Laboratory of Optic-electric Sensing and Analytical Chemistry for Life Science, Ministry of Education, Shandong Key Laboratory of Biochemical Analysis, Key Laboratory of Analytical Chemistry for Life Science in Universities of Shandong, College of Chemistry and Molecular Engineering, Qingdao University of Science and Technology, Qingdao 266042, China*

ARTICLE INFO

Article history:
Received 15 May 2020
Received in revised form 1 August 2020
Accepted 9 September 2020
Available online 10 September 2020

Keywords:
Silver nanoparticles
Graphene quantum dot nanozyme
Dual-mode biosensing
H_2O_2 response
Cancer cell recognition
Synergistic therapy

ABSTRACT

A multifunctional nanocomposite of AgNPs@GQDs is prepared by synergistic *in-situ* growth of silver nanoparticles (AgNPs) on the complex of tannic acid (TA) and graphene quantum dots (GQDs) for the construction of dual-mode biosensing platform and cancer theranostics. The nanocomposite exhibits a hydrogen peroxide (H_2O_2)-responsive degradation, in which Ag^0 is oxidized to Ag^+ along with the release of oxidized TA and GQDs. The degradation induces the decreased absorbance and enhanced fluorescence (FL) intensity due to the suppression of Förster resonance energy transfer (FRET) in AgNPs@GQDs, which is employed for colorimetric/fluorescence dual-mode sensing of H_2O_2. The intrinsic peroxidase-like activity of GQDs nanozyme can effectively catalyze the oxidation reaction, enhancing the detection sensitivity significantly. Based on the generation of H_2O_2 from the oxidation of glucose with the catalysis of glucose oxidase (GOx), this nanoprobe is versatilely used for the determination of glucose in human serum. Further, through combining the H_2O_2-responsive degradation of AgNPs@GQDs with high H_2O_2 level in cancer cells, the nanocomposites exhibit good performance in cancer cell recognition and therapy, in which the synergistic anticancer effect of Ag^+ and oxidized TA contribute to effective cell death, and the liberated GQDs are used to monitor the therapeutic effect by cell imaging.

Silver nanoparticles (AgNPs) exhibit excellent optical features including high extinction coefficient, surface-plasmon resonance (SPR) and ultraviolet-visible (UV–vis) absorption [1], which have been successfully exploited to construct various biosensing platforms with easy operation and low cost [2–5]. Moreover, AgNPs have also attracted great attention in biomedical fields due to their anticancer activity [6,7]. However, most of the previously reported AgNPs only provide colorimetric signal, which cannot be used for monitoring the therapeutic process in cells. Although fluorescent molecules can be anchored onto AgNPs to facilitate both biosensing and therapeutic monitoring, the tedious synthesis procedure is still a challenge.

Chemical reduction is the most frequently used method to prepare AgNPs [8]. Tannic acid (TA) is natural polyphenolic compound with a central glucose and 10 galloyl groups [9], not only serving as a weak reducing agent, but also participating in the antibacterial and antineoplastic process, further contributing to the therapeutic effect of AgNPs [10]. However, the weak reducing ability of TA results in the instability of AgNPs, which thus affects the analytical performance and may cause cytotoxicity to both cancer and normal cells. Therefore, it is of vital importance to exploit protective agents to stabilize the nanoparticles during the growth of AgNPs. Graphene quantum dot (GQDs) are graphene nanosheets of less than 100 nm in lateral size with various functionalized groups, which can not only be employed as probes in biosensing and bioimaging due to their satisfactory optical properties [11], but also serve as favorable reductant and stabilizer for the growth of metal nanoparticles [12]. Furthermore, GQDs are also a new class of nanozymes with intrinsic peroxidase-like activity based on the intact aromatic structure and abundant periphery carboxylic groups [13,14], which have been widely applied in biosensing, bioimaging and biomedicine [15].

Herein, a colorimetric/fluorescence dual-mode biosensing and theranostic platform is established based on the synergistic *in-situ*

* Corresponding authors.
E-mail addresses: bisai11@126.com (S. Bi), zhangxueji@szu.edu.cn (X. Zhang).

https://doi.org/10.1016/j.cclet.2020.09.013

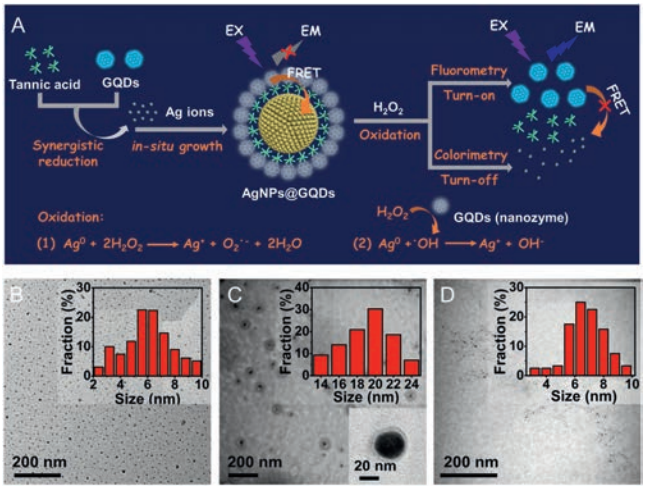

Fig. 1. (A) Schematics of synergistic *in-situ* growth of AgNPs@GQDs for dual-mode colorimetric/fluorescence sensing of H_2O_2. (B–D) TEM images and size distribution of GQDs, AgNPs@GQDs, and AgNPs@GQDs in H_2O_2 (50 μmol/L), respectively.

growth of AgNPs through one-step reduction of Ag^+ stabilized by TA-GQDs complex (Fig. 1A). TA serves as the reducing agent and GQDs can also provide reducing and stabilizing ability as well, which is partially oxidized to quinone structure (Scheme S1 in Supporting information). Due to the surface oxygen functional groups and aromatic groups, GQDs are prone to complex with TA through hydrogen bonding and π-π stacking interaction [16]. Moreover, the deprotonated amino groups on the surface of GQDs promote the electrostatic interaction between GQDs and TA under alkali condition [17]. The combination of TA and GQDs promotes the synergistic *in-situ* growth of silver nanoparticles. The assembled GQDs on the surface of AgNPs protect AgNPs@GQDs from aggregation or degradation, while the fluorescence (FL) of GQDs is quenched by AgNPs through Förster resonance energy transfer (FRET) [18]. Hydrogen peroxide (H_2O_2) will oxidize AgNPs@GQDs to Ag^+, leading to the degradation of AgNPs@GQDs along with the release of GQDs and oxidized TA ($Ag^0 + 2H_2O_2 \rightarrow Ag^+ + O_2^{\bullet-} + 2H_2O$, oxidation reaction (1)) [19]. The degradation induces the decreased absorbance and hinders the FRET process simultaneously, resulting in the recovered FL intensity of GQDs. Hence, AgNPs@GQDs are employed as dual-mode probes for sensing of H_2O_2. Furthermore, the assembled GQDs nanozyme on the surface of AgNPs provide peroxidase-like activity to catalyze the decomposition of H_2O_2 with the generation of hydroxyl radical ($^{\bullet}OH$) that has higher oxidizing ability than H_2O_2 [20]. Therefore, the oxidation degree of AgNPs@GQDs is improved effectively due to the oxidation reaction (2) ($Ag^0 + {}^{\bullet}OH \rightarrow Ag^+ + OH^-$), thus contributing to the enhanced detection sensitivity of H_2O_2.

To verify the formation mechanism of AgNPs@GQDs, a series of microscopic and spectroscopic characterizations are carried out. Transmission electron microscopy (TEM) images of GQDs demonstrate a good monodispersity with the average diameter of 6.4 nm in lateral size (Fig. 1B). As expected, the as-prepared AgNPs@GQDs exhibit well stability and excellent dispersibility, since no adhesion of nanoparticles are observed in the TEM images (Fig. 1C). Due to the hydrogen bonding, π-π stacking and electrostatic interaction, satellites assembly form with multiple GQDs surrounding AgNPs [21]. In comparison, AgNPs without the assembly of GQDs show the morphology with a little aggregation (Fig. S1 in Supporting information), which are smaller than that of AgNPs@GQDs (14–24 nm). The chemical component and formation process of AgNPs@GQDs are thoroughly verified by XPS spectra and XRD patterns (Figs. S2 and S3 in Supporting information). The Brunauer-Emmett-Teller (BET) surface areas of AgNPs@GQDs (25.3479 m^2/g) is larger than that of AgNPs (8.5552 m^2/g) due to the assembly of GQDs (Fig. S4 in Supporting information). Upon treating with H_2O_2, the characteristic nanoparticles of AgNPs@GQDs disappear, and the monodisperse nanodots with the average diameter of 6.7 nm are observed in TEM image (Fig. 1D). This suggests the H_2O_2-responsive degradation of AgNPs@GQDs, and the remaining small nanodots are corresponding to the liberated GQDs.

The as-prepared AgNPs@GQDs exhibit UV–vis absorption (λ_{max} = 412 nm), with a weak shoulder at 270 nm related to GQDs, demonstrating the formation of AgNPs under the synergistic reduction of Ag^+ by TA and GQDs (Fig. S5A in Supporting information). The FL emission of AgNPs@GQDs is quenched by AgNPs through FRET (Fig. S5B in Supporting information) due to the overlap between FL emission spectra of GQDs and UV–vis absorption spectra of AgNPs@GQDs (Fig. S5C in Supporting information). Moreover, since TA can shorten the distance between GQDs and AgNPs, the quenching efficiency can be further enhanced significantly [21]. With the increase of H_2O_2 concentration, the absorbance of AgNPs@GQDs at 412 nm decreases along with the increase of FL intensity (Figs. S6A and S6B in Supporting information), while no variation is observed in AgNPs under the same conditions (Figs. S6C and S6D in Supporting information). The optical changes of AgNPs@GQDs and AgNPs in H_2O_2 show higher sensitive response of AgNPs@GQDs than AgNPs toward H_2O_2 (Figs. 2A and B), which is probably ascribed to the assembly of GQDs nanozyme that catalyze the decomposition of H_2O_2 to generate $^{\bullet}OH$ with high redox potential (2.73 V) [22]. The oxidizing ability of $^{\bullet}OH$ is higher than that of H_2O_2, enhancing the oxidation degree of AgNPs@GQDs [23]. As a nanozyme, the kinetics data of GQDs is investigated as shown in Fig. S7 and Table S1 (Supporting information). Furthermore, the nanozyme activity of GQDs in AgNPs@GQDs is validated through the catalytic oxidation of the chromogenic substrate TMB (3,3′,5,5′-tetramethylbenzidine) in the presence of H_2O_2 [24,25]. Compared with AgNPs, the absorbance of oxTMB sharply increases with the catalysis of AgNPs@GQDs, demonstrating the enhanced catalytic activity of AgNPs@GQDs assembled with GQDs (Fig. S8 in Supporting information). After optimizing the detecting conditions (Fig. S9 in Supporting information), a turn-off colorimetry is adopted for sensing of H_2O_2, in which

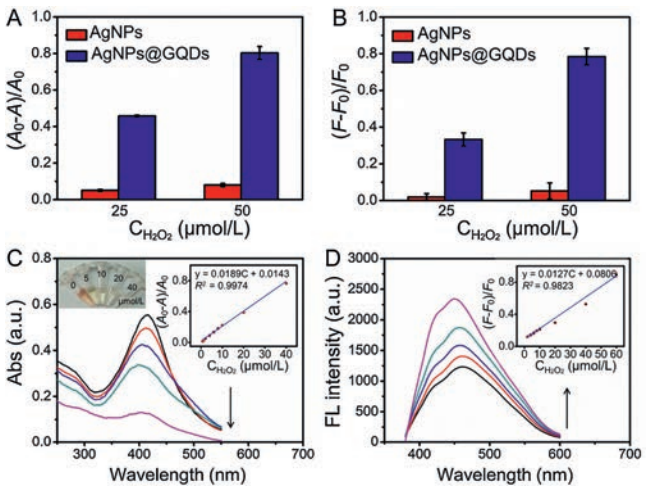

Fig. 2. (A) Absorbance and (B) FL intensity changes of AgNPs@GQDs and AgNPs in H_2O_2. (C) UV–vis absorption spectra of AgNPs@GQDs under different concentrations of H_2O_2 (0-40 μmol/L); inset: photographs of AgNPs@GQDs in the presence of H_2O_2 and linear relationship between $(A_0\text{-}A)/A_0$ *versus* H_2O_2 concentration, A_0 and A are the absorbance of AgNPs@GQDs at 412 nm in the absence and presence of H_2O_2, respectively. (D) FL emission spectra of AgNPs@GQDs under different concentrations of H_2O_2 (0-60 μmol/L); inset: linear relationship between $(F\text{-}F_0)/F_0$ *versus* H_2O_2 concentration; F_0 and F are the FL intensities of AgNPs@GQDs at 450 nm in the absence and presence of H_2O_2, respectively; the error bars represent standard deviation by means of three independent measurements.

absorbance at 412 nm decreases as the H_2O_2 concentration increases with color fading (Fig. 2C) [12]. The relative absorbance $(A_0\text{-}A)/A_0$ displays a good linear relationship with the concentration of H_2O_2 in the range of 0.08–40 μmol/L, and the detection limit is estimated to be 25 nmol/L (3σ/s, in which σ is the standard deviation for the blank solution ($n = 11$), and s is the slope of the calibration curve). As shown in Fig. 2D, the FL intensity of AgNPs@GQDs gradually increases as the concentration of H_2O_2 increases, facilitating the fabrication of turn-on FL nanosensor for H_2O_2 determination. A good linear relationship is developed between the relative FL intensity $(F\text{-}F_0)/F_0$ and H_2O_2 concentration with a range from 2−60 μmol/L and detection limit of 0.83 μmol/L (3σ/s).

Glucose oxidase (GOx) can specifically catalyze the oxidation of glucose to gluconic acid by oxygen (O_2), with H_2O_2 as a byproduct (glucose + O_2 + $H_2O \xrightarrow{GOx}$ gluconic acid + H_2O_2, reaction (3)) [26]. Combining this reaction with the degradation of AgNPs@GQDs induced by H_2O_2, the proposed dual-mode biosensing platform can be versatilely applied to glucose detection (Fig. S10A in Supporting information), in which a linear range of 0.5−50 μmol/L with detection limit of 170 nmol/L (3σ/s) is achieved from colorimetric assay (Fig. S10B in Supporting information), and a linear range of 5−100 μmol/L with detection limit of 1.31 μmol/L (3σ/s) is obtained from FL method (Fig. S10C in Supporting information), respectively. The potential interfering effects of the species frequently encountered in biological samples are tested by analyzing the absorbance response of AgNPs@GQDs toward glucose in the presence of various coexisting species. It is evident that within a ±5% error range, 100 μmol/L of the coexisting foreign species cause no interference to the detection of glucose (Fig. S11 in Supporting information). In comparison with the recently reported Ag nanomaterials-associated glucose sensing systems, our proposed nanosensor exhibits not only high sensitivity but also excellent selectivity (Table S2 in Supporting information). To evaluate the practical applicability of the AgNPs@GQDs-based nanosensor for glucose detection, glucose contents in human serum samples are determined (Table S3 in Supporting information), which are consistent with the blood glucose content in healthy human body (4–7 mmol/L) [27]. The spiking recoveries 92.89%–104.44% are achieved for glucose in the human serum samples, indicating the accuracy and reliability of the proposed method for glucose analysis.

H_2O_2 is one of the most important ROS in cells, which plays a crucial role in cell growth, proliferation, and differentiation [28]. Particularly, the higher H_2O_2 level in cells is usually associated with cancerization, since cancer cells have to generate more H_2O_2 (at a range of 50–100 μmol/L) to activate the proximal signaling pathways and support the cell proliferation [29]. Combining the H_2O_2-responsive capacity of the AgNPs@GQDs nanocomposite with high H_2O_2 level in cancer cells, the proposed nanosensor exhibits the potential in cell imaging and cancer therapy (Fig. 3A). The microenvironment of cancer cells with high H_2O_2 level stimulates the disassembly of AgNPs@GQDs and release of Ag^+, oxidized TA and GQDs. Ag^+ can cause cell death based on the induction of oxidative stress, mitochondrial damage, and autophagy [7]. Moreover, the oxidized TA is demonstrated as a potential prooxidant for anticancer, which is found to induce apoptotic death by chromosome condensation and DNA fragmentation *via* extrinsic and intrinsic activation pathways due to the formation of quinone structure [30,31]. Thus, in the proposed H_2O_2-responsive AgNPs@GQDs nanosystem, the synergistic effect of Ag^+ and oxidized TA can cause distinguished efficacy on cancer cell death and apoptosis, and the released GQDs with the restored FL can be employed as FL imaging probe to recognize cancer cells and monitor the therapeutic effect. In contrast, the low concentration of H_2O_2 in normal cells cannot induce the degradation of AgNPs@GQDs. Thus, AgNPs@GQDs hardly cause the cytotoxity to normal cells. Moreover, in normal cells the assembled GQDs prevent the direct contact between AgNPs and cells to induce cell death or apoptosis, and the FL is still quenched by AgNPs. As shown in Figs. 3B–D, the bright blue FL images are observed after treating the cancer cells (Karpas299 and HepG-2 cells) with AgNPs@GQDs, and the obvious morphological changes of the cancer cells indicate the effective therapeutic effect of AgNPs@GQDs. However, normal cells (L02 cells) are in a good state, and neither morphological changes of cells in bright field nor FL in imaging is observed. In contrast, although AgNPs have therapeutic effect on cancer cells (Karpas299 and HepG-2 cells), they also cause inevitable damage to normal cells (L02 cells), since no additional protecting agent exists in AgNPs, which will directly interact with cells to damage the cells and cannot provide any FL signal. Thus, the proposed multifunctional AgNPs@GQDs nanocomposite demonstrate as intelligent probes for cancer cell recognition and therapeutic effect.

To further evaluate the cancer cell selective therapeutic effect of AgNPs@GQDs, the cytotoxicity of cancer cells (Karpas299 and HepG-2 cells) and normal cells (L02 cells) treated with different concentrations of AgNPs@GQDs is studied *via* CCK-8 assay (Fig. 4A). As the concentration of AgNPs@GQDs increases, the viability of cancer cells (Karpas299 and HepG-2 cells) decreases gradually, while the viability of normal cells (L02 cells) remains unchanged compared with the control group without any treatment. In contrast, AgNPs induce obvious cell death on both

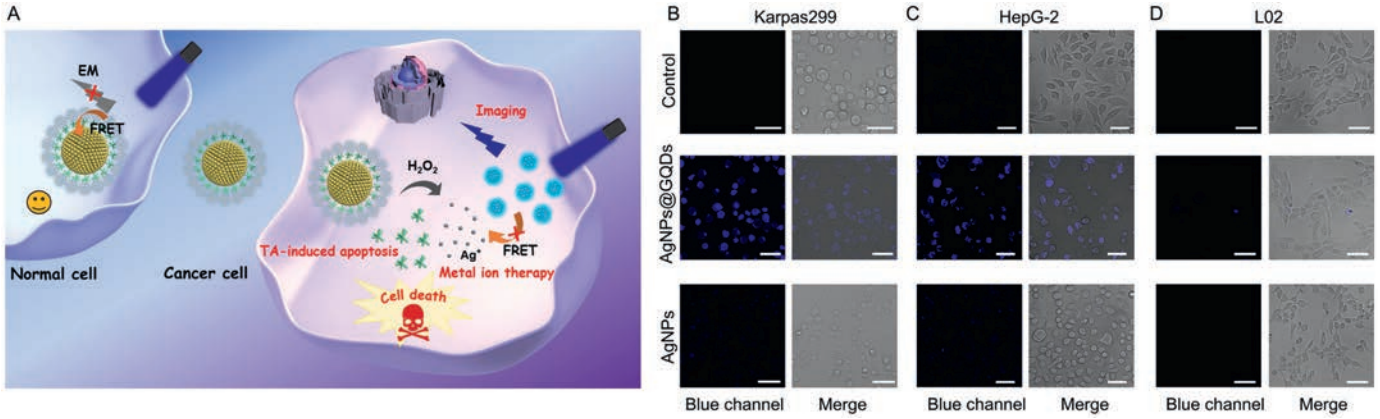

Fig. 3. (A) Schematics of cancer cell recognition and anticancer therapeutic effect of AgNPs@GQDs; confocal images of (B) Karpas299 cells, (C) HepG-2 cells and (D) L02 cells after treatment with DMEM (control), AgNPs@GQDs ($A = 0.6$) and AgNPs ($A = 0.6$) for 12 h; scale bar: 50 μm.

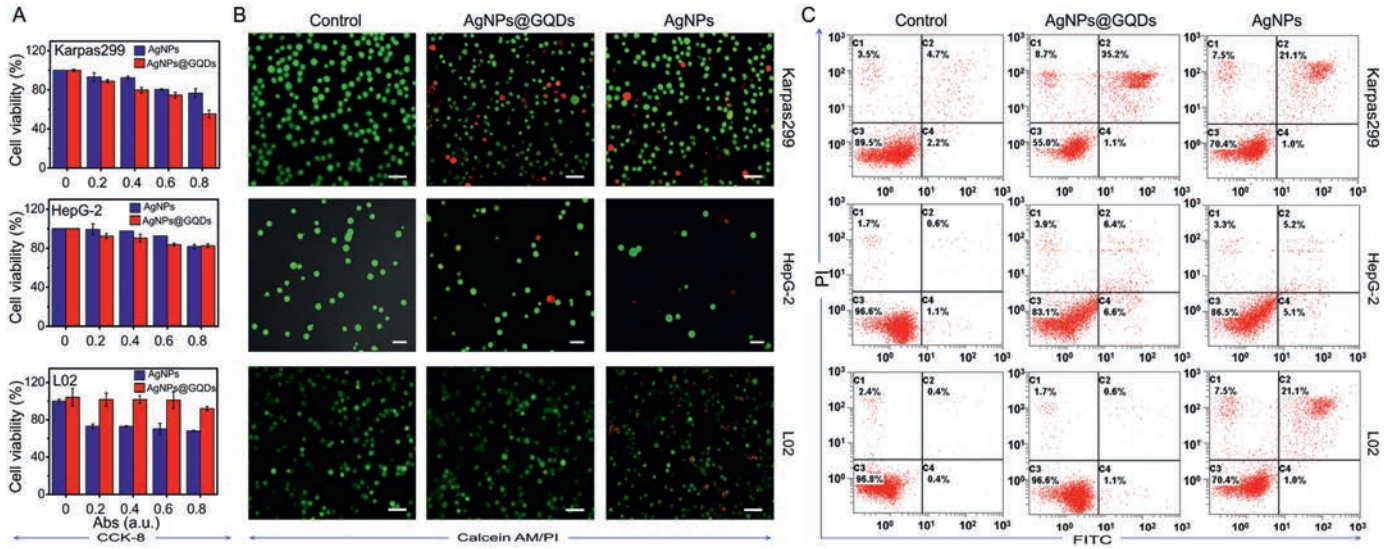

Fig. 4. Selective therapeutic effect of AgNPs@GQDs for cancer cells: (A) The viability of different cells after treated with a series concentration of AgNPs@GQDs and AgNPs for 12 h; (B) CLSM images of cells co-stained with Calcein-AM/PI and (C) flow cytometry analysis of cells co-stained with FITC-Annexin V/PI after treated with DMEM (control), AgNPs@GQDs ($A = 0.6$) and AgNPs ($A = 0.6$); the scale bars in CLSM images are 50 μm; C1, C2, C3 and C4 in flow cytometry analysis represent the regions of dead cells, late apoptotic cells, live cells and early apoptotic cells, respectively.

cancer cells (Karpas299 and HepG-2 cells) and normal cells (L02 cells). To further assess the selective killing capacities of AgNPs@GQDs, the three kinds of cells treated with AgNPs@GQDs and AgNPs are double-stained with Calcein AM (green FL) and propidium iodide (PI, red FL) to directly visualize the live and dead cells, respectively (Fig. 4B). In the AgNPs@GQDs-treated group, the cancer cells are killed and display the red FL (dead cells), while the normal cells keep their viability with exclusively green FL (live cells). However, both of the cancer cells and normal cells are killed after treated with AgNPs. Flow cytometry assay further proves the selective anticancer effect of AgNPs@GQDs, in which two dyes of FITC-Annexin V and PI are used to stain the apoptosis and necrotic cells, respectively (Fig. 4C). The results indicate that AgNPs@GQDs cause obvious death and apoptosis only in cancer cells (Karpas299 and HepG-2 cells), while hardly pose any toxicity to normal cells (L02 cells). However, in the presence of AgNPs, all of these cells can be killed with obvious death and apoptosis, especially for normal cells (L02 cells). These results demonstrate the cancer cell recognition and therapy ability of AgNPs@GQDs.

In summary, multifunctional AgNPs@GQDs with obvious UV–vis absorption and quenched FL emission have been readily synthesized by synergistic *in-situ* growth of AgNPs on TA and GQDs complex. AgNPs@GQDs exhibit H_2O_2-responsive degradation, in which Ag^0 is oxidized to Ag^+ along with the release of oxidized TA and GQDs, achieving a colorimetric/fluorescence dual-mode H_2O_2 nanosensor. Significantly, the intrinsic peroxidase-like activity of GQDs nanozyme in AgNPs@GQDs can effectively catalyze the oxidation reaction, which facilitates to enhance the detection sensitivity of H_2O_2. Moreover, this AgNPs@GQDs based nanosensor is used for dual-mode analysis of glucose in human serum samples. Furthermore, the AgNPs@GQDs nanoprobes exhibit good performance in cell imaging for cancer cell recognition and therapy. Therefore, this multifunctional nanocomposite holds great potential in biosensing and biomedicine, and provides theoretical basis for the construction of clinical theranostic nanoplatforms.

Declaration of competing interest

The authors report no declarations of interest.

Acknowledgments

This work was supported by the National Natural Science Foundation of China (Nos. 21722505 and 21705086), the Special Funds of the Taishan Scholar Program of Shandong Province (No. tsqn20161028), the Youth Innovation Technology Program of Shandong Province (No. 2019KJC029), the Natural Science Foundation of Shandong Province (No. ZR2017JL009), the Collaborative Innovation Program of Jinan (No. 2018GXRC033), the Open Project of Shandong Key Laboratory of Tumor Marker Detection Technology (Nos. KLDTTM2019-4, KLDTTM2019-5) and the Open Project of Chemistry Department of Qingdao University of Science and Technology (No. QUSTHX201928).

Appendix A. Supplementary data

Supplementary material related to this article can be found, in the online version, at doi:https://doi.org/10.1016/j.cclet.2020.09.013.

References

[1] H. Kang, J.T. Buchman, R.S. Rodriguez, et al., Chem. Rev. 119 (2019) 664–699.
[2] M. Liu, L. Zhang, Y. Hua, et al., Anal. Chem. 89 (2017) 9552–9558.
[3] H. Liu, S. Li, L. Feng, et al., J. Hazard. Mater. 388 (2020) 121798.
[4] Z. Sun, N. Zhang, Y. Si, et al., Chem. Commun. 50 (2014) 9196–9199.
[5] J. Fu, Z. Zhang, G. Li, Chin. Chem. Lett. 30 (2019) 285–291.
[6] J. Lin, Y. Liu, H. Wu, et al., Small 14 (2018) e1703711.
[7] Y.F. Zhang, Y.C. Yang, S.S. Jiang, et al., Mater. Horiz. 6 (2019) 169–175.
[8] N.G. Bastús, F. Merkoçi, J. Piella, V. Puntes, Chem. Mater. 26 (2014) 2836–2846.
[9] T. Liu, M.K. Zhang, W.L. Liu, et al., ACS Nano 12 (2018) 3917–3927.
[10] X.R. Song, S.H. Li, H. Guo, et al., Adv. Sci. 5 (2018) 1801201.
[11] H.T. Lu, W.J. Li, H.F. Dong, M.L. Wei, Small 15 (2019) 19.
[12] S. Chen, X. Hai, X.W. Chen, J.H. Wang, Anal. Chem. 86 (2014) 6689–6694.
[13] Y. Hu, X.J. Gao, Y. Zhu, et al., Chem. Mater. 30 (2018) 6431–6439.
[14] J. Wu, X. Wang, Q. Wang, et al., Chem. Soc. Rev. 48 (2019) 1004–1076.
[15] H. Wang, C.Q. Liu, Z. Liu, et al., Small 14 (2018) 8.
[16] B. Sinduja, S.A. John, RSC Adv. 6 (2016) 59900–59906.
[17] J. Ren, F. Weber, F. Weigert, et al., Nanoscale 11 (2019) 2056–2064.
[18] J.L. Ma, B.C. Yin, X. Wu, B.C. Ye, Anal. Chem. 89 (2017) 1323–1328.
[19] S.G. Liu, S. Mo, L. Han, et al., Anal. Chim. Acta 1055 (2019) 81–89.
[20] H.J. Sun, N. Gao, K. Dong, et al., ACS Nano 8 (2014) 6202–6210.
[21] L. Wang, J. Zheng, Y. Li, et al., Anal. Chem. 86 (2014) 12348–12354.
[22] Y. Zhang, L. Qiang, Y. Yuan, et al., Environ. Sci.: Nano 5 (2018) 1191–1199.

[23] H.J. Sun, Y. Zhou, J.S. Ren, X.G. Qu, Angew. Chem. Int. Ed. 57 (2018) 9224–9237.
[24] S. Bi, S. Yue, S. Zhang, Chem. Soc. Rev. 46 (2017) 4281–4298.
[25] J. Zheng, D. Song, H. Chen, et al., Chin. Chem. Lett. 31 (2020) 1109–1113.
[26] L.H. Fu, C. Qi, J. Lin, P. Huang, Chem. Soc. Rev. 47 (2018) 6454–6472.
[27] R. Pandey, S.K. Paidi, T.A. Valdez, et al., Acc. Chem. Res. 50 (2017) 264–272.
[28] H. Ding, Y. Cai, L. Gao, et al., Nano Lett. 19 (2018) 203–209.
[29] T. Liu, W. Liu, M. Zhang, et al., ACS Nano 12 (2018) 12181–12192.
[30] P.K.B. Nagesh, E. Hatami, P. Chowdhury, et al., Cancers 10 (2018) 68.
[31] S. Azam, N. Hadi, N.U. Khan, S.M. Hadi, Toxicol. In Vitro 18 (2004) 555–561.